5

MaximumMIMO — Millimeter Wave Line-of-Sight Spatial Multiplexing

Xiaohang Song, Wolfgang Rave, Gerhard Fettweis

Vodafone Chair Mobile Communications Systems, Technische Universität Dresden

Tim Hälsig, Berthold Lankl

Chair of Communication Systems, Universität der Bundeswehr München

Darko Cvetkovski, Eckhard Grass

Department of Computer Science, Humboldt-Universität zu Berlin

CONTENTS

DOI: 10.26127/BTUOpen-5911

5.1 Introduction

Fixed wireless communication systems are a cost-efficient solution for flexible and rapid front-/backhaul deployments. Technologies exploiting dual polarization, carrier aggregation, and higher order modulation schemes have been employed for enhancing their throughput. In order to support the massive traffic increase coinciding with the evolving wireless networks worldwide, novel wireless backhaul solutions with an additional degree of freedom are required. In this chapter, we will focus one such technology called Line-of-Sight (LoS) Multiple-Input-Multiple-Output (MIMO) systems, which can achieve high spectral efficiency by parallel data stream transmission over the same time-frequency resources.

5.1.1 Conventional Backhaul Technologies

Standard backhaul solutions achieve their high data rates through large bandwidths, e.g., by using carrier aggregation, high modulation alphabets, i.e., obtaining a high link signal-to-noise ratio (SNR) with directive antennas, and polarization multiplexing. With these techniques, microwave systems currently available on the market can provide up to 4 Gbit/s for LoS backhaul links [190]. Lack of bandwidth is one key reason that limits the throughput. Millimeter wave (mmWave) bands have been proposed as new frequency region for such systems to solve this issue. For example, around 60 GHz, IEEE 802.11ay [191] regulates six channels of 2.16 GHz bandwidth each, for outdoor wireless backhaul, and also allows channel bonding mechanisms for four of those channels. Employing bonding at 60 GHz and using 16-QAM (quadrature amplitude modulation), a single stream transmission can achieve 28.16 Gbit/s at a distance of 0.8 meter [192].

High path loss [193] is one limitation of utilizing mmWave links over longer distances. However, with directive antennas or beamforming technologies, this drawback can be overcome. For example, with the help of highly directive antennas of 55.1 dBi, the authors of [194] demonstrated a single stream mmWave transmission at 240 GHz over a distance of 850 m. Under the LoS dominant scenario, an error vector magnitude (EVM) of -11.9 dB was achieved with a 32 Gbaud 4-QAM modulation, yielding a data rate of 64 Gbit/s.

In order to increase the data rate even further, multiple transmit streams using the same time-frequency resource, e.g., by employing cross-polarized antennas with strong polarization selectivity as supported by IEEE 802.11ay, are also considered for backhaul applications. Experimental results [195] have shown that 60 GHz antennas can have a cross polarization discrimination factor of approximately 20 dB under LoS conditions. However, polarization multiplexing is typically limited to a maximum number of parallel streams of two, therefore limiting the gain that can be achieved. Another polarization

related technique, called multiplexing based on different orbital angular momentum (OAM) modes [196], can increase the number of parallel streams, but requires more complex antenna designs.

5.1.2 Benefits and Challenges of the LoS MIMO Technique

Compared to polarization multiplexing, LoS MIMO offers greater multiplexing capabilities. In contrast to the prevailing interpretation of the channel matrices in LoS communication being rank one [197, 198], spatial multiplexing with sub-channels having approximately equal quality can be exploited in LoS conditions for certain antenna arrangements [199, 200]. This is independent of the polarization multiplexing and can be used in addition to it. Assuming spherical wave propagation, highly orthogonal channel matrices can be obtained with widely spaced antennas [201, 202, 203, 204]. In 2017, the European Electronic Communications Committee (ECC) took notice of this and started to consider the usage of LoS MIMO technologies in fixed service links [205]. Furthermore, using LoS MIMO at millimeter wave frequencies, a very low energy per bit, in the order of 10 pJ/bit, can be achieved [206]. LoS MIMO was also shown to be suitable in combination with low resolution quantization [207, 208, 209], which can further improve the energy efficiency.

However, the performance of a LoS MIMO system is highly dependent on the antenna topology. The general topology solution from a unified viewpoint is unknown, and the known optimal arrangements in the literature are rather independently derived and contain restrictions on their array planes, e.g., [210, 211]. Moreover, operating at mmWave frequencies with wideband signals introduces additional challenges. On one hand, high path loss is a limiting factor in terms of the received signal power. On the other hand, high symbol rates and a relatively high number of antennas create challenges for the signal processing in such systems [212, 213]. Especially the design of low complexity algorithms for compensating hardware imperfections, including synchronization, at mmWave frequencies [192, 214, 215] is a demanding task.

In this work, we focus on antenna topologies and signal processing schemes to effectively handle the complexity challenges in LoS MIMO communications. Considering the antenna topology, we aim for a general solution of optimal arrangements on any arbitrarily curved surface. Moreover, we study the antenna topologies with which the system gains more streams and improved received signals. Considering the signal processing, we look for low complexity schemes that can effectively compensate the hardware impairments and can support a large number of antennas. We describe estimation, equalization, and synchronization techniques that are focused on the LoS MIMO backhaul scenario, and prove their viability in a demonstrator setup. General system design requirements, such as achievable throughput and actual measured behavior of the LoS MIMO channel, are also treated.

5.2 LoS MIMO Basics

Instead of exploiting spatial multiplexing based on different LoS/NLoS paths, LoS MIMO approaches have shown the existence of spatial multiplexing gains within a single path direction [199, 200]. By using the spherical wave propagation model, LoS MIMO systems with special antenna typologies can be designed to overcome the famous key-hole effect which leads to the rank of channel matrices to be one using planar wave propagation. Relying on structured interference, particular antenna topologies not only restore the full rank of the channel matrices, but also provide a *condition number* being one in the ideal cases [201, 202, 203, 204]. In theory, using the same time-frequency resource and co-polarized antennas, parallel streams with approximately equal sub-channel quality can then be transmitted within the LoS path direction.

5.2.1 Parallel Antenna Topologies

In this part, we introduce the state-of-the-art works on antenna topology with a focus on the arrays that are arranged in parallel. Here, we modify the classic symmetric LoS MIMO system with equal antenna numbers and spacings at Tx and Rx in [203] to a more general asymmetric setup, which would generalize the parallel solutions.

Physical Channel Model: Let us assume that the transmitter (Tx) and the receiver (Rx) are two uniform linear arrays (ULA) parallel to the y-axis at $x = 0$ and $x = D$, respectively, see Fig. 5.1. Here, the variable D denotes the transmit distance. The antennas Tx-1 and Rx-1 at bottom ends of the two arrays are both located on the x-axis with $y = 0$. A carrier frequency f_{c} with a corresponding wavelength $\lambda = c/f_{\mathrm{c}}$ is used by the transceiver arrays. Furthermore, the Tx and Rx consist of N_{t} and N_{r} isotropic antenna elements with spacings d_{t} and d_{r}, respectively, and $\lambda \ll d_{\mathrm{t}}, d_{\mathrm{r}} \ll D$. Moreover, let us use $D_{n_{\mathrm{r}}n_{\mathrm{t}}}$ to denote the distance between the n_{r}-th receive element and the n_{t}-th transmit element. The associated channel matrix is written as

$$\mathbf{H} = \alpha \underbrace{\mathbf{H}_{\mathrm{LoS}}}_{\substack{\text{Phase} \\ \text{Couplings}}}, \tag{5.1}$$

where α indicates the common channel gain between all transmit-receive antenna pairs[1]. $\mathbf{H}_{\mathrm{LoS}} \in \mathbb{C}^{N_{\mathrm{r}} \times N_{\mathrm{t}}}$ describes the relative phase shifts between all antenna pairs with unit magnitude entries. The works in [216, 217] show that a spherical wave model is more accurate and has even positive consequences compared to the conventional approach using a planar-wave model,

[1] As shown later, under the assumptions that $\lambda \ll d_{\mathrm{t}}, d_{\mathrm{r}} \ll D$, the $D_{n_{\mathrm{r}}n_{\mathrm{t}}}$ values will differ from each other by certain fractions of λ, which are negligible for calculating the channel gain.

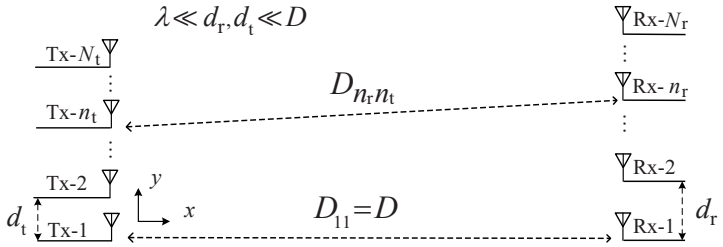

Figure 5.1
A LoS MIMO system with parallel uniform linear arrays. From [218]

by sidestepping the keyhole channel problem, for widely spaced antennas. Describing the propagation with the spherical wave model, the phase coupling between Rx-n_r and Tx-n_t can be expressed as

$$\{\mathbf{H}_{\text{LoS}}\}_{n_r n_t} = e^{-j\frac{2\pi}{\lambda}\cdot(D_{n_r n_t} - D)}. \tag{5.2}$$

where the common phase term $2\pi D/\lambda$ is neglected for simplification of the discussion later.

Uniform Linear Antenna Arrangements: As can be seen from (5.2), if $D_{n_r n_t}$ values differ from each other by certain fractions of λ, the phase shifts of different antenna pairs will differ by certain fractions of 2π. This motivates the antenna topology design that leads to spatial multiplexing in strong LoS conditions.

Let us first examine the geometry property of $D_{n_r n_t}$. Without loss of generality, we assume $N_t \leqslant N_r$ first. Describing the location of Tx-n_t and Rx-n_r in a Cartesian coordinate system as $(0, (n_t{-}1)d_t)$ and $(D, (n_r{-}1)d_r)$, respectively, we obtain

$$D_{n_r n_t} = \sqrt{D^2 + [(n_r{-}1)d_r - (n_t{-}1)d_t]^2} \approx D + \frac{[(n_r{-}1)d_r - (n_t{-}1)d_t]^2}{2D}, \tag{5.3}$$

where the approximation follows from the first order Taylor expansion of the square root using $d_t, d_r \ll D$, e.g., $(1{+}a)^{1/2} \approx 1{+}a/2$ s.t., $a \ll 1$. Moreover, the n_t-th column of the matrix $\mathbf{H}_{\text{LoS}}$ can be found as

$$\mathbf{h}_{n_t} = \exp\Big(j\frac{2\pi}{\lambda}D\Big) \cdot \Big[\exp\Big(-j\frac{2\pi}{\lambda}D_{1n_t}\Big),\ \ldots,\ \exp\Big(-j\frac{2\pi}{\lambda}D_{N_r n_t}\Big)\Big]^T. \tag{5.4}$$

In order to have $\mathbf{H}_{\text{LoS}}$ orthogonal, the inner product of any two different columns $\mathbf{h}_{n_t}$ and $\mathbf{h}_{n_t'}$ has to be equal to zero, i.e.,

$$\mathbf{h}_{n_t'}^H \mathbf{h}_{n_t} \propto \frac{\sin(\frac{\pi d_r d_t}{\lambda D} N_r (n_t - n_t'))}{\sin(\frac{\pi d_r d_t}{\lambda D}(n_t - n_t'))} = 0, \tag{5.5}$$

One solution to (5.5) can be found as

$$d_r d_t = \lambda D / N_r, \tag{5.6}$$

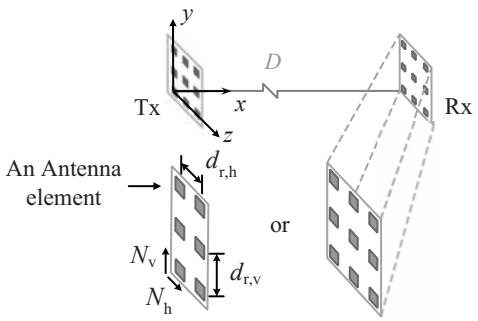

Figure 5.2
A LoS MIMO system with parallel uniform rectangular arrays of $N = N_v \cdot N_h$ elements on each side. From [219] © 2015 IEEE

which is also a joint condition on the antenna spacings at Tx and Rx. Similarly, if $N_t > N_r$, the rows of $\mathbf{H}_{LoS}$ are orthogonal to each other when $d_r d_t = \lambda D/N_t$. In addition, we would like to note that other solutions to (5.5) exist and the one in (5.6) always provides the shortest antenna spacing. Other solutions for a given N_r should also have the numerator in (5.5) being zero, while avoiding the denominator being zero for all n_t, n_t' that $n_t \neq n_t'$.[2] For example, when $N_t = N_r = 2$, more solutions are found with

$$d_r d_t = \nu \lambda D/N_r, \quad \nu \in \{1, 3, 5, 7, ...\}. \tag{5.7}$$

With a symmetric setup having smallest array aperture, the Rx and Tx of a LoS MIMO system have an equal number of antennas, i.e., $N \triangleq N_t = N_r$ and an equal antenna spacing, i.e.,

$$d_{LoS} \triangleq d_r = d_t = \sqrt{\frac{\lambda D}{N}}. \tag{5.8}$$

Furthermore, the phase coupling matrix $\mathbf{H}_o$ from this optimal arrangement has the property

$$\mathbf{H}_o^H \cdot \mathbf{H}_o = N \cdot \mathbf{I}_N, \tag{5.9}$$

which was our design goal, and which is equivalent to a condition number of one, i.e., $\kappa(\mathbf{H}_o) = 1$. The entries of $\mathbf{H}_o$ in an optimally arranged symmetric system with parallel ULAs satisfy $\{\mathbf{H}_o\}_{n_r n_t} \approx e^{-j\pi(n_r - n_t)^2/N}$, considering (5.3).

Uniform Rectangular Antenna Arrangements: As shown in [203], the orthogonality of LoS MIMO channel can also be achieved with parallel

[2] Otherwise, the L'Hospital's rule would apply, and it gives a non-zero inter product between $\mathbf{h}_{n_t'}$ and $\mathbf{h}_{n_t}$.

uniform rectangular arrays (URAs), see Fig. 5.2. For a setup of $N = N_{\mathrm{h}} \cdot N_{\mathrm{v}}$ antennas at both transceiver and receiver, the phase coupling matrix $\mathbf{H}_{\mathrm{LoS}}$ can then be factorized into a Kronecker product of two phase coupling matrices of ULAs along two orthogonal directions as

$$\mathbf{H}_{\mathrm{LoS}} = \mathbf{H}_{\mathrm{LoS,h}} \otimes \mathbf{H}_{\mathrm{LoS,v}}\,, \tag{5.10}$$

where $\mathbf{H}_{\mathrm{LoS,h}}$ and $\mathbf{H}_{\mathrm{LoS,v}}$ denote two phase coupling matrices of ULAs with N_{h} and N_{v} elements, respectively. Therefore, the horizontal and vertical antenna spacings can be independently designed. Thus, the optimal antenna spacing $d_{\mathrm{t,h}},\ d_{\mathrm{r,h}},\ d_{\mathrm{t,v}}$ and $d_{\mathrm{r,v}}$ of URAs in the horizontal and vertical directions would satisfy [211]

$$d_{\mathrm{t,h}} \cdot d_{\mathrm{r,h}} = \frac{\lambda D}{N_{\mathrm{h}}},\quad d_{\mathrm{t,v}} \cdot d_{\mathrm{r,v}} = \frac{\lambda D}{N_{\mathrm{v}}}, \tag{5.11}$$

and such designs lead to orthogonal matrices again as $\mathbf{H}_{\mathrm{LoS}}^{H} \cdot \mathbf{H}_{\mathrm{LoS}} = N \cdot \mathbf{I}_N$ or, equivalently, $\kappa\left(\mathbf{H}_{\mathrm{LoS}}\right) = 1$ [220].

Non-parallel Arrangements: Above, we have discussed the antenna arrangements on two parallel lines or planes. However, the orthogonality can also be achieved with arrangements on tilted non-parallel lines/planes. In [211], the authors present non-parallel linear and planar solutions. Specifically, the planar array solutions were only known for limited planar rotation directions and the arrays are restricted to URA.

Relation with Rayleigh Distance: In antenna theory, Rayleigh distance is defined as the boundary between the Fresnel (Radiating Near-Field) and Fraunhofer (Far-Field) regions of the space surrounding an antenna [183]. The Rayleigh distance is not uniquely defined, but it is proportional to $d_{\mathrm{ant}}^2/\lambda$ as

$$D_{\mathrm{Ray}} \propto \frac{d_{\mathrm{ant}}^2}{\lambda}, \tag{5.12}$$

where d_{ant} is the largest linear dimension of the antenna. Since the LoS MIMO system uses widely spaced antennas at far distances, we use the original definition of the Fresnel and Fraunhofer regions for individual antennas in this work including the discussions above. However, it is noticed that, if one considers the complete Tx/Rx array as an isolated source of electromagnetic radiation, the LoS MIMO system with symmetric setup would operate at each others' Rayleigh distance. For asymmetric Tx/Rx arrays of very different dimensions, the smaller array would operate at the Fresnel region of the larger one and the spherical wave model should be kept.

LoS MIMO Channel Capacity: In LoS MIMO communication with optimal/near-optimal antenna arrangement, the Tx should expect the subchannels are of equal/nearly equal quality. In high SNR regions that are feasible in backhaul communications, this leads to equal power allocation. Then, the capacity of LoS MIMO systems follows the well-known 'convenient general capacity expression' [221, 222] as

$$C_{\mathrm{MIMO}}^{\mathrm{LoS}} = \log_2 \det(\mathbf{I}_{N_{\mathrm{r}}} + \frac{\gamma}{N_{\mathrm{t}}} \cdot \mathbf{H}_{\mathrm{LoS}} \mathbf{H}_{\mathrm{LoS}}^{H}), \tag{5.13}$$

where the SNR at each received antenna $\gamma = \alpha^2 P_{\mathrm{T}}/\sigma_{\mathrm{n}}^2$. For comparison, the channel capacity of LoS SISO communication, which is an AWGN channel with the same sum power as the MIMO system, is given by [223] as

$$C_{\mathrm{SISO}}^{\mathrm{LoS}} = \log_2\left(1 + \frac{\alpha^2}{\sigma_{\mathrm{n}}^2} \cdot P_{\mathrm{T}}\right) = \log_2\left(1 + \gamma\right), \tag{5.14}$$

where γ denotes the SNR as $\gamma = \alpha^2 P_{\mathrm{T}}/\sigma_{\mathrm{n}}^2$. For the LoS MIMO systems with an equal number of antennas at Tx and Rx, $N_{\mathrm{t}} = N_{\mathrm{r}} = N$ and in the ideal case with full channel orthogonality, we obtain a linear increase in the capacity with the number of antennas, i.e., $C_{\mathrm{MIMO}}^{\mathrm{LoS}} = N \cdot C_{\mathrm{SISO}}^{\mathrm{LoS}}$.

5.2.2 MmWave LoS MIMO as a Backhaul Technique

LoS MIMO point-to-point communication at millimeter waves is a promising technique for achieving multi-Gigabit data rates for wireless backhaul systems. Considering the achievable high rank channel matrices and the associated good condition numbers in (5.9), the LoS spatial multiplexing can multiply the data rates of SISO backhaul links. In addition, due to the small wavelength in (5.8), mmWave wireless communication systems also have reasonable antenna sizes. This may help to utilize such spatial multiplexing gains in practical systems, beyond the power gains achievable with beamforming. As an example for 60 GHz systems ($\lambda \simeq 5\,\mathrm{mm}$), (5.8) shows that two linear arrays of a length about 1 m each allow 4 parallel streams for 100 m front-/backhaul communication. The concept of applying LoS MIMO at mmWave frequencies is verified by channel measurements provided in [220], which shows a good agreement between theory and practice. However, high path loss is one critical limitation of utilizing the mmWave band [193]. Having directive antennas and/or applying beamforming for array power gains are widely considered in overcoming the short range limitation [224]. In this part, we investigate the potential of systems deploying the aforementioned LoS spatial multiplexing on top of the array power gain.

A two-level hierarchical MIMO system was reported in our earlier work in [219]. On the higher level, this is a MIMO system that contains N_{t} and N_{r} subarrays at Tx and Rx, respectively, to exploit the spatial multiplexing

Table 5.1
60 GHz Backhaul Examples [219], $D = 100\,\mathrm{m}$, bandwidth 2.16 GHz. From [219] © 2015 IEEE

Super-array Size	N	SNR [dB]	Bandwidth Efficiency	Achievable Rate
7.5 mm × 7.5 mm	1	18.3	6.1 bits/s/Hz	13.2 Gb/s
0.50 m × 0.50 m	4	18.3	24.4 bits/s/Hz	52.8 Gb/s
0.82 m × 0.82 m	9	18.3	54.9 bits/s/Hz	118.8 Gb/s
1.06 m × 1.06 m	16	18.3	87.6 bits/s/Hz	211.2 Gb/s

gain in deterministic channels. In this work, the array of several widely spaced subarrays is named 'super-array'. The lower level refers to the architecture of the subarrays with densely packed antennas that would provide fixed beamforming gain to compensate for the path loss. With the link budget provided in [219], the spectral efficiency has the potential of reaching one hundred bits per channel use (BPCU). Considering the degradation of the system due to effects like RF impairments and possible high peak-to-average power ratio (PAPR) values, the system should be designed in a reasonable size with high throughput including some redundancy. Further considering that high SNR values require hardware impairments to be low, which may leads high costs, system setups with N from 4 to 16 in Tab. 5.1 are then the most interesting ones at 100 meters in setting up links with a throughput in the order of 100 Gbit/s. The maximum width and height of the arrays are not larger/much larger than 1 meter. Meanwhile, they are operating at SNR values without ultra-high quality requirements on the hardware, which may potentially reduce the cost. Most importantly, these setups can reach link budgets in the order of 100 Gbit/s, i.e., at least about 52.8 Gbit/s using one 2.16 GHz channel at 60 GHz, which can be further scaled by using other resources. For example, the maximum data rates in the table can be doubled by expanding the system with cross-polarized antennas, but a signal-to-interference-plus-noise ratio (SINR) ceiling should be expected due to the non-ideal polarization separation. Furthermore, IEEE 802.11ay [191] allows channel bonding mechanisms for four of those 2.16 GHz channels around 60 GHz, which can scale the throughput as well.

Here, we would like to note that the existence of secondary paths/reflections in the channel may further enhance the spatial multiplexing in fixed wireless applications. Motivated by the robustness of LoS spatial multiplexing against transmit directions, the LoS spatial multiplexing due to the structured phase couplings can be introduced to other path directions. This would further increase the throughput of fixed wireless links. We direct the interested readers to our earlier publication in [213] for more details.

As described above, LoS MIMO systems rely on the array geometry and the corresponding orthogonality of the phase relationships between antennas. This may present a challenge for the practical implementation of these systems and shall therefore be considered. If the optimal spacing criterion is not fulfilled, e.g., due to implementation tolerances, the orthogonality of the channel is degraded. In spite of that in practical scenarios it is difficult to exactly achieve orthogonality, it has been shown that the system is robust in terms of system capacity against moderate translation and rotation changes [203, 207], when one uses moderate numbers of antennas. This robustness property of the LoS spatial multiplexing will be explained via a mathematical model proposed in Section 5.3.

5.3 LoS MIMO Channel Equalization

This section focuses on a general channel factorization model and the LoS MIMO channel tap equalization. Especially, comparing with two conventional linear estimator, we shows a novel algorithm, namely sequential channel equalization (SCE), for the equalization under dominant-LoS channels. The equalization is applied in a reverse order w.r.t. the channel factorization model. The major results of this chapter have been presented in part in [225, 207, 226, 227].

5.3.1 LoS MIMO Channel Factorization

In [225], we have first derived the channel factorization model for LoS MIMO communication as a product of three matrices, i.e.,

$$\mathbf{H}_{\text{LoS}} = \mathbf{D}_{\parallel,\text{r}} \cdot \mathbf{H}_{\perp} \cdot \mathbf{D}_{\parallel,\text{t}}. \tag{5.15}$$

The two outer diagonal matrices $\mathbf{D}_{\parallel,\text{r}}$ and $\mathbf{D}_{\parallel,\text{t}}$, respectively on the right and left hand side. For different realizations of the LoS MIMO channel under near optimal arrangements, the diagonal elements of $\mathbf{D}_{\parallel,\text{r}}$ and $\mathbf{D}_{\parallel,\text{t}}$ have very different phases but have the same magnitude. According to the mathematical interpretation given in [225], we showed that $\mathbf{D}_{\parallel,\text{r}}$ and $\mathbf{D}_{\parallel,\text{t}}$ are contributed by displacements along the transmit direction and are normalized to the wavelength λ. Due to the fact that λ is relatively small at high frequencies, the realization of $\mathbf{D}_{\parallel,\text{r}}$ and $\mathbf{D}_{\parallel,\text{t}}$ is sensitive to displacement errors along the transmit direction. However, with further mathematical analysis, we showed that $\mathbf{D}_{\parallel,\text{r}}$ and $\mathbf{D}_{\parallel,\text{t}}$ do not influence the channel capacity and singular values. Subsequently, from a projection point of view, we concluded in [225] that the capacity of a strong point-to-point LoS MIMO channel is much less variant with respect to the displacements along the transmit direction.

The aperture of the array in broadside relative to transmit direction determines the performance. The displacements on this plane, i.e., the plane perpendicular to the transmit direction, would lead to different realizations on $\mathbf{H}_{\perp}$. However, the realizations of $\mathbf{H}_{\perp}$ are much less sensitive to displacement errors, since those errors are normalized by a relative large value $\sqrt{\lambda D}$. The discussions above would lead to three interesting conclusions as given in [225]. First, the optimized solutions for the 2D LoS MIMO array are also the best solutions for point-to-point 3D LoS MIMO systems. Second, the optimal antenna arrangements on any curved surface can be easily obtained via mapping the corresponding broadside arrangement to the surface. As an example, 1D or 2D antenna arrangements that compensate the degradation from the tilt angles are discussed and presented. Finally, it is important to note that the spatial multiplexing gain of LoS MIMO systems is shown to be robust mathematically, since the realization of $\mathbf{H}_{\perp}$ is robust and $\mathbf{D}_{\parallel,\text{r}}$, $\mathbf{D}_{\parallel,\text{t}}$ do not influence the channel capacity.

As an evolution to this factorization model, in [227], we have shown that the middle term in (5.16) has a structure of inverse discrete Fourier transform (IDFT). Further denoting the IDFT matrix of N points as $\mathbf{W}_{\text{IDFT-}N}$, the channel can be factorized in another form as

$$\mathbf{H}_{\text{LoS}} = \tilde{\mathbf{D}}_{\parallel,\text{r}} \cdot (\mathbf{W}_{\text{IDFT-}N} + \tilde{\mathbf{H}}_{\Delta}) \cdot \tilde{\mathbf{D}}_{\parallel,\text{t}}, \tag{5.16}$$

where $\tilde{\mathbf{D}}_{\parallel,\text{r}}$ and $\tilde{\mathbf{D}}_{\parallel,\text{t}}$ are two diagonal matrices with a fixed phase shift to the diagonal elements of $\mathbf{D}_{\parallel,\text{r}}$ and $\mathbf{D}_{\parallel,\text{t}}$, respectively. Furthermore, as discussed in [226, 207, 227], we must note that $\tilde{\mathbf{H}}_{\Delta}$ is contributed by the displacement errors on the plane that is perpendicular to the transmit direction and those errors are normalized by a relative large value $\sqrt{\lambda D}$. Considering applications with near optimal arrangement, the entries of $\tilde{\mathbf{H}}_{\Delta}$ are then of small values, e.g., $\left|\{\tilde{\mathbf{H}}_{\Delta}\}_{n_{\text{r}}n_{\text{t}}}\right| \ll 1$.

5.3.2 Conventional Linear Signal Estimation Algorithms

In this part, let us first exam the linear system model for LoS MIMO communication and then discuss two commonly known linear estimation algorithms. Next in Section 5.3.3, we extend the discussion by introducing a novel successive channel equalization algorithm [227] considering the channel factorization introduced in Section 5.3.1.

We restrict the discussion on signal estimation to linear algorithms due to their low complexity, which is a crucial aspect for ultra wideband signal processing in wireless backhaul systems. Exhaustive search algorithms, like the maximum likelihood estimation [228], may require higher complexity (exponential complexity in N) than necessary especially for systems operating at high SNR regions. This complexity argument also holds for interference cancellation algorithms, like the successive interference cancellation using sorted QR decomposition [229], due to their multi-layer structures. Linear estimation is therefore a straightforward, low complexity strategy to find the estimates.

To simplify the discussion, we assume the common channel gain α in (5.1) to be one. Therefore, the general signal transfer model for this frequency flat channel can be presented with $\mathbf{H}_{\text{LoS}}$ as

$$\mathbf{y} = \mathbf{H}_{\text{LoS}} \cdot \mathbf{x} + \mathbf{n}, \tag{5.17}$$

where $\mathbf{x} \in \mathbb{C}^{N\times 1}$ and $\mathbf{y} \in \mathbb{C}^{N\times 1}$ are the transmitted signal vector and the received signal vector, respectively. The noise vector $\mathbf{n}$ is modeled with i.i.d. complex white Gaussian random entries that are circularly symmetric, $\mathbf{n} \sim \mathcal{CN}(\mathbf{0}, \sigma_{\text{n}}^2 \cdot \mathbf{I}_N)$. Furthermore, it is assumed that the power is allocated uniformly at streams with i.i.d. Gaussian signaling $\mathbf{x} \sim \mathcal{CN}(\mathbf{0}, \sigma_{\text{s}}^2 \cdot \mathbf{I}_N)$. In addition, assuming perfect channel knowledge at Rx with synchronized transceivers, we express the estimate $\hat{\mathbf{x}}$ on $\mathbf{x}$ with an equalizer $\mathbf{W}$ as $\hat{\mathbf{x}} = \mathbf{W}\cdot\mathbf{y}$.

Minimum Mean Square Error (MMSE) Estimation: The channel equalizer $\mathbf{W}_{\text{MMSE}}$ is determined by minimizing the mean squared error between the transmitted signal and the estimated signal $\mathbf{W}_{\text{MMSE}} =$

$\arg\min_{\mathbf{W}} \mathbb{E}[||\hat{\mathbf{x}} - \mathbf{x}||_F^2]$, and is formulated as

$$\mathbf{W}_{\text{MMSE}} \triangleq (\mathbf{H}_{\text{LoS}}^H \mathbf{H}_{\text{LoS}} + \frac{\sigma_{\text{n}}^2}{\sigma_{\text{s}}^2} \mathbf{I}_N)^{-1} \mathbf{H}_{\text{LoS}}^H. \tag{5.18}$$

This solution is the optimal linear estimator with the mean square error as its cost criteria [228].

Zero-Forcing (ZF) Equalization: The ZF algorithm defines an equalizer with the pseudo-inverse of the channel matrix as

$$\mathbf{W}_{\text{ZF}} \triangleq (\mathbf{H}_{\text{LoS}}^H \mathbf{H}_{\text{LoS}})^{-1} \mathbf{H}_{\text{LoS}}^H. \tag{5.19}$$

One of the main drawbacks in implementing ZF based equalization is that, if the channel matrix is ill-conditioned, the algorithm suffers from noise enhancement. However, for optimal and even near-optimal arrangements, the channel in LoS MIMO communication is expected to be well-conditioned. Given that the $||\mathbf{y} - \mathbf{H}_{\text{LoS}} \cdot \mathbf{x}||_F^2$ is convex, this solution is also the least squares estimator for $\mathbf{x}$ as $\frac{\partial ||\mathbf{y} - \mathbf{H}_{\text{LoS}} \cdot \mathbf{x}||_F^2}{\partial \mathbf{x}}\Big|_{\mathbf{x}=\mathbf{W}_{\text{ZF}}\mathbf{y}} = 0$.

In the next part, we will consider ZF as our baseline algorithm based on the following arguments. First, for communication systems with high SNR values typical for backhaul scenarios, i.e., $\sigma_{\text{s}}^2 \gg \sigma_{\text{n}}^2$, the MMSE estimation can be well approximated by the ZF estimation. Secondly, in the low SNR region, the effective SNR values under optimal arrangements are also the same for both algorithms, since $\mathbf{H}_{\text{LoS}}$ is orthogonal. This makes both ZF estimation and MMSE estimation being system capacity achieving solutions, although the biased MMSE estimation provides less estimation errors than the unbiased ZF estimation in general. Eventually, ZF requires no information on the SNR value, which makes the implementation simpler.

5.3.3 Sequential Channel Equalization

For practical backhaul systems with massive deployments, the displacement errors of LoS MIMO antenna arrangements should be taken into consideration. Although the coherence time of the channel is expected to be very long due to the quasi-deterministic scenarios, the variability of the deployment requires flexible algorithms. The conventional methods, i.e., straightforward implementations of ZF and MMSE algorithms, do not consider the special property of LoS MIMO channels and require N^2 complex number multiplications per received symbol (not considering the SNR estimation associated with MMSE). In [227], we proposed to use an algorithm with three steps considering the property of the LoS MIMO matrix $\mathbf{H}_{\text{LoS}}$. The number of multiplications required by the proposed method is only increasing approximately linearly w.r.t. small values of N in full digital implementation. We briefly summarize the key ideas as follows.

Processing Architecture: Since the channel is expected to be full rank,

the channel equalization can be performed in the reverse order w.r.t. the channel factorization in (5.16), yielding an equalizer structure equivalent to ZF equalization as

$$\mathbf{W}_{\mathrm{ZF}} = \tilde{\mathbf{D}}_{\parallel,\mathrm{t}}^{-1}(\mathbf{W}_{\text{IDFT-}N} + \tilde{\mathbf{H}}_{\Delta})^{-1}\tilde{\mathbf{D}}_{\parallel,\mathrm{r}}^{-1}. \tag{5.20}$$

Motivated by this, a novel three-step equalization method is proposed in a reverse order. Three matrix multiplications are performed sequentially with the outer ones being diagonal matrices. Therefore, the design of SCE follows the ZF criterion, but can be considered as a low-complexity approximation to the ZF based algorithm in (5.20). The SCE matrix $\mathbf{W}_{\mathrm{sce}}$ is modeled as

$$\mathbf{W}_{\mathrm{sce}} \triangleq \mathbf{D}_2 \cdot \mathbf{W}_{\mathrm{fix}} \cdot \mathbf{D}_1, \tag{5.21}$$

where $\mathbf{D}_1$ and $\mathbf{D}_2$ are two diagonal matrices. For different antenna topology realizations, the two matrices $\mathbf{D}_1$ and $\mathbf{D}_2$ are chosen accordingly to the resulting $\mathbf{H}_{\mathrm{LoS}}$. Considering ULAs at Tx and Rx with N elements each, $\mathbf{W}_{\mathrm{fix}}$ can be implemented with a fixed N-point discrete Fourier transform (DFT) matrix

$$\mathbf{W}_{\mathrm{fix}} = \mathbf{W}_{\text{DFT-}N}, \tag{5.22}$$

where $\mathbf{W}_{\text{DFT-}N}$ denotes a DFT matrix of N-points. Furthermore, considering URAs at Tx and Rx with $N = N_{\mathrm{v}} \cdot N_{\mathrm{h}}$ elements each, the $\mathbf{W}_{\mathrm{fix}}$ can be implemented with $\mathbf{W}_{\mathrm{fix}} = \mathbf{W}_{\text{DFT-}N_{\mathrm{h}}} \otimes \mathbf{W}_{\text{DFT-}N_{\mathrm{v}}}$, if one considers the channel factorization model for URA systems [227]. The design of SCE follows the ZF criterion, but its performance is impaired by the interference caused by $\tilde{\mathbf{H}}_{\Delta}$. Since the zero-forcing based algorithm is capable of offering an interference-free solution, the objective function of setting $\{\mathbf{D}_1, \mathbf{D}_2\}$ can be stated as the 'distance' between $\mathbf{W}_{\mathrm{sce}}$ and the ZF baseline algorithm $\mathbf{W}_{\mathrm{ZF}}$. For detailed discussions on finding practical $\{\mathbf{D}_1, \mathbf{D}_2\}$ with only knowledge/estimate on $\mathbf{H}_{\mathrm{LoS}}$, we refer the readers to our original publication [227].

Complexity Reduction: In practice, those DFT operations can be implemented with the Fast Fourier Transform (FFT) based structures of reduced complexity. Thus, the usage of $\mathbf{W}_{\mathrm{fix}}$ for equalizing $(\mathbf{W}_{\text{IDFT-}N} + \tilde{\mathbf{H}}_{\Delta})$ brings the benefit of saving computational complexity at the cost of slightly lower SINR caused by $\tilde{\mathbf{H}}_{\Delta}$. This comes from the fact that, within certain displacement error ranges, the entries of $\tilde{\mathbf{H}}_{\Delta}$ are of small values $\left|\{\tilde{\mathbf{H}}_{\Delta}\}_{n_{\mathrm{r}}n_{\mathrm{t}}}\right| \ll 1$. Being a good trade off between complexity and robustness against displacement errors, the proposed algorithm can be applied to the LoS MIMO systems with uniform linear or rectangular arrays using digital or analog equalization [227]. By considering the usage of the Winograd butterfly and Butler DFT-matrices, the number of multiplications in both digital and analog implementations of the proposed solution is increasing approximately linearly w.r.t. the number of antennas, while the complexity of the state-of-the-art designs, like zero-forcing, exhibits quadratic growth.

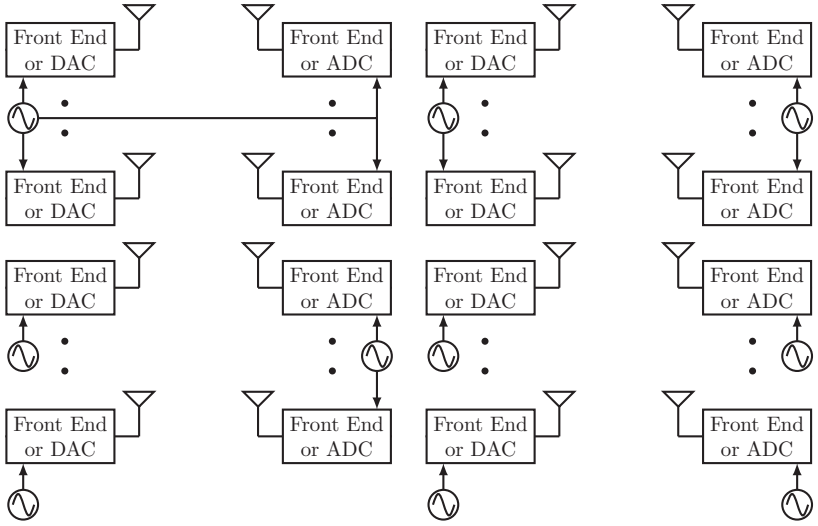

Figure 5.3
The four basic MIMO oscillator configurations. From [230]

5.4 Synchronization for LoS MIMO Systems

MIMO systems are typically comprised of several transmitter and receiver front ends, in order to generate and capture the different streams. With multiple front ends, the question arises of how to synchronize them. For most communication systems, two basic frequencies are required per front end for transmission. The first one is the sampling frequency, sometimes also referred to as the timing, which defines the symbol rate at the transmitter, and the sampling frequency at the receiver. In the ideal case of a shared oscillator between all MIMO transmitter and receiver front ends, and no fixed sampling shift due to the channel, the receiver samples the correct time instances of the continuous time signal, where the symbols are located. In most practical cases, sharing an oscillator between the transmitted and receiver is not feasible, and localizing the correct symbol timings has to be achieved by other means. The second frequency required for wireless transmission is the carrier frequency. As in the sampling frequency case, when a frequency is shared, downconversion of the received signal is ideal, up to time invariant phase shifts due to the channel, and the symbols can be correctly identified. If the frequency is not shared, time variant phase shifts exist on the received signal, which have to be compensated before the signal can be properly demodulated.

In general, it is not necessary for MIMO systems to share the same sampling or carrier frequency among all transmitters or receivers to synchronize the system. It has been shown that by using different digital signal process-

ing techniques, the frequency differences can be estimated and compensated [231, 213, 230]. In the general MIMO case, multiple independent oscillators may exist in the system. Even though all of the oscillators in the system may have the same nominal frequency, due to aging, temperature and mechanical variations, the actual frequencies that are generated have to be assumed slightly different. The frequency differences are called sampling frequency offset (SFO) and carrier frequency offset (CFO), respectively. Figure 5.3 gives an overview of all possible basic oscillator configurations for MIMO systems. They are applicable to sampling and carrier frequency generation independently. Different setups require different levels of complexity for frequency difference estimation and compensation. In the most general case of independent carrier and sampling frequency generation for each transmitter and receiver front end, one has to deal with $2 \cdot N_\mathrm{r} \cdot N_\mathrm{t}$ frequency differences [232], generated by $2 \cdot N_\mathrm{r} + 2 \cdot N_\mathrm{t}$ deviations from the nominal frequency.

5.4.1 Correlation Based Estimators

When the frequency differences are relatively small, correlation based estimators using uncorrelated training sequences from the different transmitters were shown to be a viable solution in the literature, see [233, 234, 213, 230]. The channel impulse response estimate associated with the n_rth receive antenna, on which low complexity frequency difference estimators can be based, is modeled as

$$\hat{\mathbf{h}}_{L,n_\mathrm{r}}[k] = \mathbf{X}_\mathrm{T}^H \cdot \mathbf{y}_{L_\mathrm{R},n_\mathrm{r}}[k], \tag{5.23}$$

where $\hat{\mathbf{h}}_{L,n_\mathrm{r}}[k]$ is a vector containing the channel impulse responses of length L at time k, $\mathbf{X}_\mathrm{T}$ is a matrix containing the training signals, and $\mathbf{y}_{L_\mathrm{R},n_\mathrm{r}}[k]$ is the received signal vector of length L_R at time k. Based on two or more of these channel estimates, separated by L_E samples, the carrier frequency differences can be estimated with

$$\boldsymbol{\Delta}\hat{\boldsymbol{\Phi}}[k] = \begin{bmatrix} e^{j\cdot\frac{1}{L_\mathrm{E}}\left(\arg\left(\hat{\mathbf{h}}^T_{\mathrm{C},L_\mathrm{C},1}[k+L_\mathrm{E}]\right)-\arg\left(\hat{\mathbf{h}}^T_{\mathrm{C},L_\mathrm{C},1}[k]\right)\right)} \\ e^{j\cdot\frac{1}{L_\mathrm{E}}\left(\arg\left(\hat{\mathbf{h}}^T_{\mathrm{C},L_\mathrm{C},2}[k+L_\mathrm{E}]\right)-\arg\left(\hat{\mathbf{h}}^T_{\mathrm{C},L_\mathrm{C},2}[k]\right)\right)} \\ \vdots \\ e^{j\cdot\frac{1}{L_\mathrm{E}}\left(\arg\left(\hat{\mathbf{h}}^T_{\mathrm{C},L_\mathrm{C},N_\mathrm{r}}[k+L_\mathrm{E}]\right)-\arg\left(\hat{\mathbf{h}}^T_{\mathrm{C},L_\mathrm{C},N_\mathrm{r}}[k]\right)\right)} \end{bmatrix}, \tag{5.24}$$

where $\boldsymbol{\Delta}\hat{\boldsymbol{\Phi}}[k]$ is the matrix containing the carrier frequency differences between all transmitters and receivers.

The lowest complexity estimator for the sampling frequency differences, given that the impact of multipath components is sufficiently attenuated by a squaring operation, is obtained by calculating a single dth DFT value of the magnitude variation of the channel estimate compared with a reference pulse,

where $d = \left\{2, \ldots, \left\lfloor \frac{L}{2Q} \right\rfloor \right\}$. The estimator can be written as

$$\begin{aligned}\Delta\hat{\phi}_{n_\mathrm{r}n_\mathrm{t}}[k] = \frac{1}{2\pi}\cdot\frac{L}{d-1}\cdot\Bigg(&\arg\left(\mathcal{F}_d\left\{\left|\hat{h}_{n_\mathrm{r}n_\mathrm{t}}[k,l]\right|^2\right\}\right)\\ &-\arg\left(\mathcal{F}_d\left\{\left|\mathrm{sinc}\left[\pi\frac{l-L/2}{Q}\right]\right|^2\right\}\right)\Bigg)\end{aligned} \tag{5.25}$$

$$\begin{aligned}= \frac{1}{2\pi}\cdot\frac{L}{d-1}\cdot\Bigg(&\arg\left(\sum_{l=0}^{L-1}\left|\hat{h}_{n_\mathrm{r}n_\mathrm{t}}[k,l]\right|^2\cdot e^{-j2\pi\cdot\frac{l}{L}\cdot(d-1)}\right)\\ &-\arg\left(\sum_{l=0}^{L-1}\left|\mathrm{sinc}\left[\pi\frac{l-L/2}{Q}\right]\right|^2\cdot e^{-j2\pi\cdot\frac{l}{L}\cdot(d-1)}\right)\Bigg),\end{aligned} \tag{5.26}$$

where $\mathcal{F}_d\{\cdot\}$ computes the dth DFT component, Q is the oversampling factor, and $\hat{h}_{n_\mathrm{r}n_\mathrm{t}}[k,l]$ is the lth channel tap at time k, e.g., $\hat{h}_{n_\mathrm{r}n_\mathrm{t}}[k,0] = \hat{h}_{\mathrm{LoS},n_\mathrm{r}n_\mathrm{t}}[k]$. It should be visible that the lower limit of d is chosen as two, since the first DFT value ($d = 1$) can not give a useful estimate for the sampling phase difference. The second argument term in (5.26) is a fixed constant for a given L, d, and Q. For certain parameter combinations, alignments, and oscillator setups, it may also be simplified [235, 236]. Other estimators, which may have improved performance when the multipath is more significant, are very similar but require at least two impulse response estimates [230].

It was thus shown that based on channel impulse response estimates, the frequency differences for sampling and carrier can be estimated with relatively low complexity by observing the variations that occur in the estimates over time. For the carrier frequency differences, the phase differences of the impulse response estimates are computed, while for the sampling frequency differences, the magnitude variations are used.

5.4.2 Combining Equalization and Synchronization

In order to properly decode the transmitted data, the frequency differences have to be compensated in conjunction with the MIMO equalization that was previously discussed in Section 5.3. It can be shown that the compensation of the frequency differences can be separated from the standard time invariant MIMO equalization [213, 230]. An equalization structure that can achieve this task for the most general setup with fully independent oscillators, is given in Figure 5.4. It is seen that the frequency differences can be compensated in parallel before and after equalization, according to their contribution from the transmitter and receiver front ends. The compensation simplifies, when other oscillator setups are used [231, 230]. It is important to note that only the frequency differences were estimated in the previous section. However, in order to use the low complexity equalizer that was just described, the differences

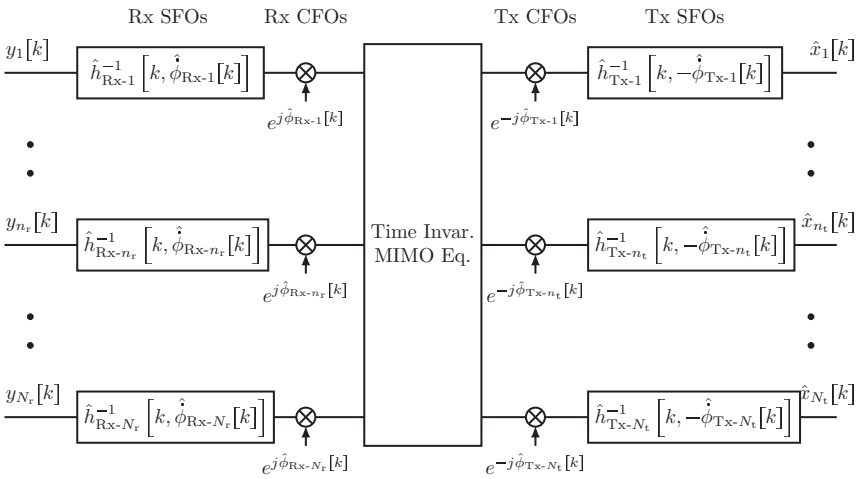

Figure 5.4
Basic equalization setup compensating multiple frequency differences and a time invariant MIMO channel. From [230]

should be separated into transmitter and receiver contribution, which can be done with a simple rank-one matrix decomposition [213, 230].

5.4.3 Adaptive Equalization

Instead of separately estimating and compensating the frequency differences, another approach that can be taken to perform equalization and synchronization is to consider the complete MIMO channel as a linear time varying filter. The task is then to reverse the characteristic of that filter, by estimating and tracking its inverse characteristic, given that it exists. This goal can be achieved by using adaptive filters in a decision directed equalization configuration. Since MIMO systems are of high dimensionality, a simple adaptive filter is required for a practical implementation. The least mean squares (LMS) algorithm is such a low complexity adaptive filter, which works well in time varying environments. An adaptive equalizer, based on LMS, can be written as

$$\hat{\mathbf{x}}[k] = \mathbf{W}_{\text{AE}}[k]\mathbf{y}_{L_{\text{R}}}[k]. \tag{5.27}$$

The update of the equalization matrix $\mathbf{W}_{\text{AE}}[k]$ is given as

$$\mathbf{W}_{\text{AE}}[k+1] = \mathbf{W}_{\text{AE}}[k] - \mu \cdot \mathbf{e}[k]\mathbf{y}^H_{L_{\text{R}}}[k], \tag{5.28}$$

where selecting the step size μ and the initialization of the equalization filter $\mathbf{W}_{\text{AE}}[0]$ is important, in order to ensure convergence and good tracking performance. Especially initialization is important in order for the DD approach

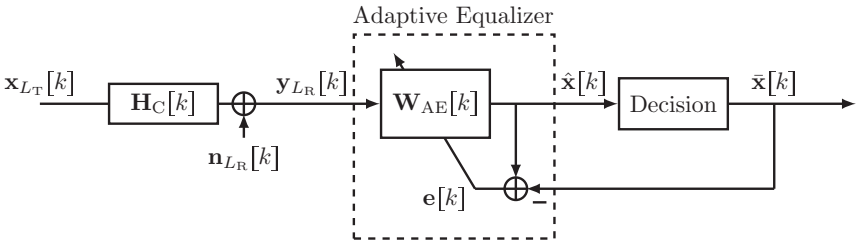

Figure 5.5
Basic working principle of adaptive equalization, i.e., adapting the equalizer $\mathbf{W}_\mathrm{AE}[k]$ based on the observed error signal $\mathbf{e}[k]$ which contains the difference between the estimated signal $\hat{\mathbf{x}}[k]$ from the equalizer output and the decided values $\bar{\mathbf{x}}[k]$ of those symbols. From [230]

to work. The error signal is defined by

$$\mathbf{e}[k] = \hat{\mathbf{x}}[k] - \bar{\mathbf{x}}[k], \tag{5.29}$$

with $\bar{\mathbf{x}}[k]$ being the decision based on the estimate $\hat{\mathbf{x}}[k]$. The equations (5.27), (5.28), and (5.29) are the only things that need to be implemented for a DD time varying adaptive MIMO equalizer, dealing with all channel impairments, based on the LMS principle. The basic configuration can be seen in Figure 5.5.

Important aspects of the adaptive equalizer are the convergence and tracking behavior, as well as the error performance. They depend on the time variation in the channel, the equalizer length, and the correlation properties of the input signals, and can be influenced by the proper selection of μ. Depending on the information available, optimal solutions for μ can be computed for different cases [237, 230]. A good solution for most cases, given that the LoS MIMO channel has a low condition number and using a feedforward equalizer, is given by

$$\mu_\mathrm{F} = \frac{4}{3} \cdot \frac{1}{\sigma_{y_m}^2 \cdot N_\mathrm{r} L_\mathrm{R}},$$

where $\sigma_y^2 \approx N_\mathrm{t} \cdot \sigma_x^2$ is the power of the received signal in each front end. Given more frequency selective channels, or a LoS tap with higher condition number, μ should be selected somewhat lower than this suggestion.

Figure 5.6 shows the convergence and equalization/tracking performance for a simulated example setup. A pure LoS MIMO channel, i.e., $L = L_\mathrm{R} = 1$, with $N_\mathrm{r} = N_\mathrm{t} = 4$ antennas, different condition numbers, and being only affected by CFOs is considered. Modulation with 16-QAM symbols was used, and the highest carrier frequency difference in the system is $\max(|\arg\{\mathbf{\Delta\Phi}[k]\}|) = 0.12°$, which is to be understood in degree per symbol. For a symbol period of 1 ns, this gives approximately a frequency difference of 300 kHz, which is a high value for typical millimeter wave systems [234, 230]. The step size μ_F was chosen for most of the results. For the convergence case,

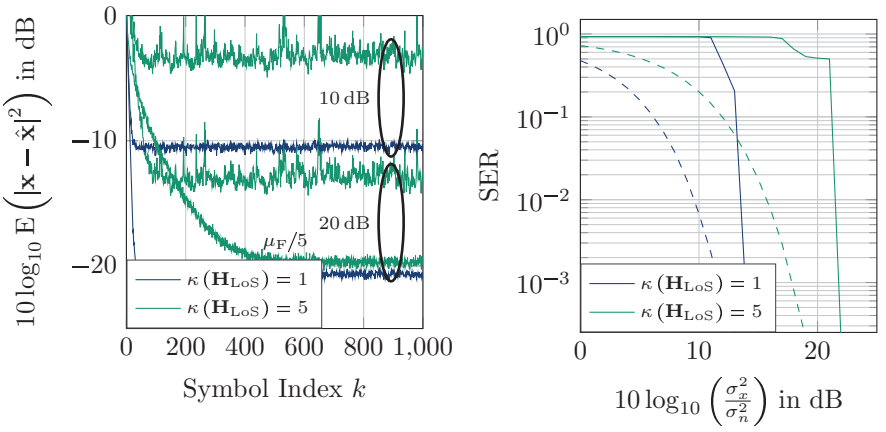

Figure 5.6
Adaptive equalization results for a pure LoS MIMO system with $L = L_\mathrm{R} = 1$, $N_\mathrm{r} = N_\mathrm{t} = 4$, and for different condition numbers using μ_F. Maxmimum frequency difference between any transmitter and receiver is 0.12 °/symbol. From [230]
Left: Convergence MSEs over time during training for different SNRs.
Right: SER for different SNRs during data transmission. The dashed curves correspond to a system without frequency differences and where the receiver has perfect channel knowledge.

two SNRs were considered, and the symbols are assumed perfectly known at the receiver. It is seen that convergence is fast in the orthogonal LoS MIMO channel case, and that the mean squared errors (MSEs) are similar to the SNR. For the non orthogonal channel case, the convergence times and MSEs are increased. However, using $\mu_\mathrm{F}/5$, similar steady state MSE can be achieved. The symbol error rate (SER) results are computed with the same setup, but based on a converged equalizer state, where the decisions $\bar{\mathbf{x}}[k]$ are used for adaptation of the equalizer. The dashed curves correspond to the same setup without frequency differences, and with perfect knowledge of the channel using $\mathbf{W}_\mathrm{ZF}$. The cliff like behavior for adaptive equalization is due to the fact that a certain SNR region needs to be reached, where most of the symbol decisions are correct, and where the equalizer then starts to adapt properly. In these SNR regions, the gap compared to the reference equalizer is less than 3 dB.

5.5 Baseband Processing Architectures

In order to satisfy the throughput demands in the range of 100 Gbit/s for the upcoming wireless networks, highly efficient transmission schemes need to be utilized. Employing multiple antennas provides an additional degree of freedom in the system design that can boost the capacity of wireless links. As discussed in Section 5.1.2, transmitting an independent data stream from each antenna in a spatial multiplexing scheme using the same time-frequency resources yields ultra-high spectral efficiency, under the assumption of a fully orthogonal channel that is provided by the LoS MIMO geometry. Designing a baseband processing architecture that can inherently support the highly parallel and wideband processing of the individual streams is therefore one of the key research points. Furthermore, the applied channel estimation, synchronization and foremost MIMO equalization algorithms need to exhibit a low complexity to be feasible for practical implementation. The transmit processing for a spatial multiplexing system mainly consists of the coding and modulation of the independent data streams and the frame composition by insertion of training sequences. As the MIMO transmitter structure is well known in literature and fairly simple, we focus our investigations on the receiver design, which involves significantly higher complexity and multiple challenges in the separation of the MIMO streams. In this section we evaluate two different approaches for the baseband processing architecture for the proposed LoS MIMO system and compare them in terms of computational complexity.

5.5.1 Receiver Baseband Architectures

Depending on the wireless system application, two different modulation schemes can be generally considered: multi-carrier modulation, where data is modulated onto multiple orthogonal frequency sub-carriers, and single-carrier (SC) modulation, where the data symbols are modulated using the complete bandwidth. The former method, also referred to as Orthogonal Frequency Division Multiplexing (OFDM), is widely used in IEEE 802.11 compatible nodes for wireless access networks operating in the sub-6 GHz carrier frequency range. By modulating data onto multiple and mutually orthogonal sub-carriers in the frequency band, the frequency-selective radio channel is reduced to a flat channel, where equalization can be performed in the frequency domain by a simple complex multiplication. When considering which modulation scheme to apply for mmWave communications, however, there are several issues that need to be considered. Foremost, mmWave radio channels are known to be highly directive due to the high propagation losses and therefore mainly flat, whereas OFDM is more suitable for rich-scattering channels. Furthermore, OFDM is highly sensitive to carrier frequency offsets and phase noise which impair the sub-carrier orthogonality, which may be a limiting

factor for its application in mmWave. Lastly, OFDM yields a high PAPR of the transmit signal that leads to inefficient use of the power amplifier. On the other hand, single-carrier modulation would lead to a more efficient baseband architecture, also allowing for a higher power amplifier dynamic range due to the lower PAPR compared to OFDM. Therefore, assuming a mainly frequency-flat mmWave radio channel, we have based our system design on single-carrier modulation with time-domain equalization.

The receiver-side processing of the streams in a spatial multiplexing scheme can be inherently performed in parallel, before and after the single-tap LoS MIMO equalization which is needed for stream separation, as depicted in Figure 5.7. This presents a scalable concept, where multiple s.c. baseband processing lanes can be instantiated depending on the number of employed antennas/streams. In that regard, the computational complexity of each of the processing sections is listed in Table 5.2. The analysis is made for a reasonable number of antennas (between 2 and 16), for which it was shown in Table 5.1 that a data rate in the order of 100 Gbit/s can be achieved. As the largest complexity lies within the LoS MIMO equalization, it is of practical interest that we apply sub-optimal but lower-complexity linear equalization schemes. If we compare the complexity of the standard ZF scheme to the proposed SCE approach in Section 5.3.3, we can conclude that SCE requires significantly less operations and scales approximately linearly with the number of antennas, whereas ZF scales only quadratically. This stems from the fact that SCE relies on a fixed equalizer matrix whereas only the diagonal matrices $\mathbf{D}_1$ and $\mathbf{D}_2$ are adjusted. In terms of their performance, in [227] it was experimentally demonstrated that it is comparable for a 2×2 LoS MIMO system.

5.5.2 Computational Complexity Analysis

As a baseline comparison for the proposed lane-based receiver architecture, the joint synchronization and adaptive decision-directed least mean squares LMS (DD-LMS) equalization approach can be considered, with its complexity given in the lower part of Table 5.2. This approach is optimal as compared to performing the synchronization, LoS single-tap equalization and intersymbol interference (ISI) cancellation in separate stages, as shown in Figure 5.7. The performance of DD-LMS was compared to SCE in [213] for a filter length of $L = 7$, where both were shown to perform roughly the same. The complexity of DD-LMS however, grows exponentially with the number of antennas N. If we compare the total computational cost of the lane-based vs. joint approach, we can conclude that the lane-based architecture with SCE for the LoS MIMO equalization both scales better and is more computationally efficient. Therefore, we can summarize that this is the desired approach for the design of practically implementable LoS MIMO receiver architectures.

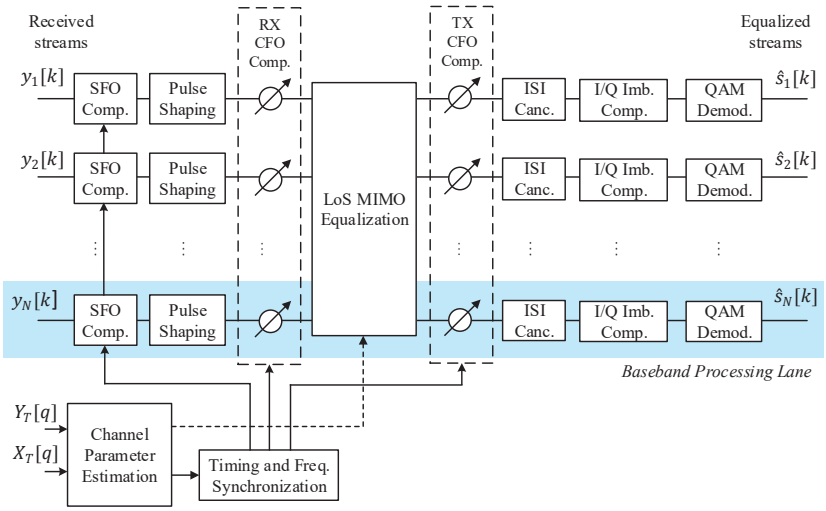

Figure 5.7
Proposed receiver baseband architecture with linear LoS MIMO equalization and parallel lane-based processing of the received streams. From [213] © 2018 IEEE

5.6 Channel Measurements and Demonstration

In order to verify the LoS MIMO concept at mmWave carrier frequencies, channel measurements were performed using an experimental 60 GHz 4×4 MIMO setup. A point-to-point link was set up between the top floor of two neighbouring buildings at a range of 21.1 m as depicted in Figure 5.8(a), in a scenario typical for wireless backhaul applications. The goal of the experimental measurements was two-fold: to characterize the properties and rank of the LoS MIMO channel and to evaluate the achievable equalizer performance for the given system setup. In the following subsections, the methodology and obtained results from the measurements are described.

5.6.1 mmWave LoS MIMO Experimental Setup

A hardware-in-the-loop approach was used to conduct the experimental measurements, with the system setup shown in Figure 5.9. The transmit waveforms were pre-compiled and repetitively generated by an arbitrary waveform generator (AWG) to the baseband inputs of the transmitting analog front-

Table 5.2
Computational cost in number of multiplications for lane-based receiver architecture with linear equalization vs. joint processing with decision-directed LMS equalization, for a filter length of $L=3$.

	Section		$N=2$	$N=4$	$N=9$	$N=16$
Lane-based Processing Architecture	CSI Estimation		0.3	1.1	6.1	21.2
	CFO Compensation		8	16	36	64
	LoS MIMO Tap Equalization	ZF	4	16	81	256
		SCE	0	0	6	0
	ISI Suppression		6	12	27	48
	I/Q Imb. Comp.		6	12	27	48
	Total	**ZF**	**24.3**	**57.1**	**177**	**437**
		SCE	**20.3**	**41.1**	**102**	**181**
DD-LMS	Channel Equalization		24	96	486	1546
	Equalizer Updating		26	100	495	1552
	Total		**50**	**196**	**981**	**3088**

ends. The baseband outputs of the receiving analog front-ends were then captured by a real-time oscilloscope (RTO) for further offline post-processing. Off-the-shelf 60 GHz analog front-ends were used for the transmission, equipped with 20 dBi horn antennas to provide a sufficient SNR for the given link range. The antennas on both ends were symmetrically set up in uniform rectangular arrays resulting in the setup depicted in Figure 5.8(b,c).

5.6.2 LoS MIMO Channel Estimation Results

One of the major goals of the experimental measurements was to verify the conditioning of optimally arranged LoS MIMO channels and its correspondence to theory. As discussed in Section 5.2, there are multiple possible antenna spacings that lead to an orthogonal/near-orthogonal channel for a LoS MIMO setup, given by (5.7). In Figure 5.10 the inverse of the condition number of the LoS MIMO channel matrix is plotted for a range of different spacings that is of practical interest for the used experimental setup. Spacings for which $1/\kappa(\mathbf{H}_{\mathrm{LoS}}) \approx 1$ would lead to a near-orthogonal, i.e., well-conditioned channel and vice versa, $1/\kappa(\mathbf{H}_{\mathrm{LoS}}) \approx 0$ would lead to an ill-conditioned channel, i.e., a channel with keyhole effect. From the sev-

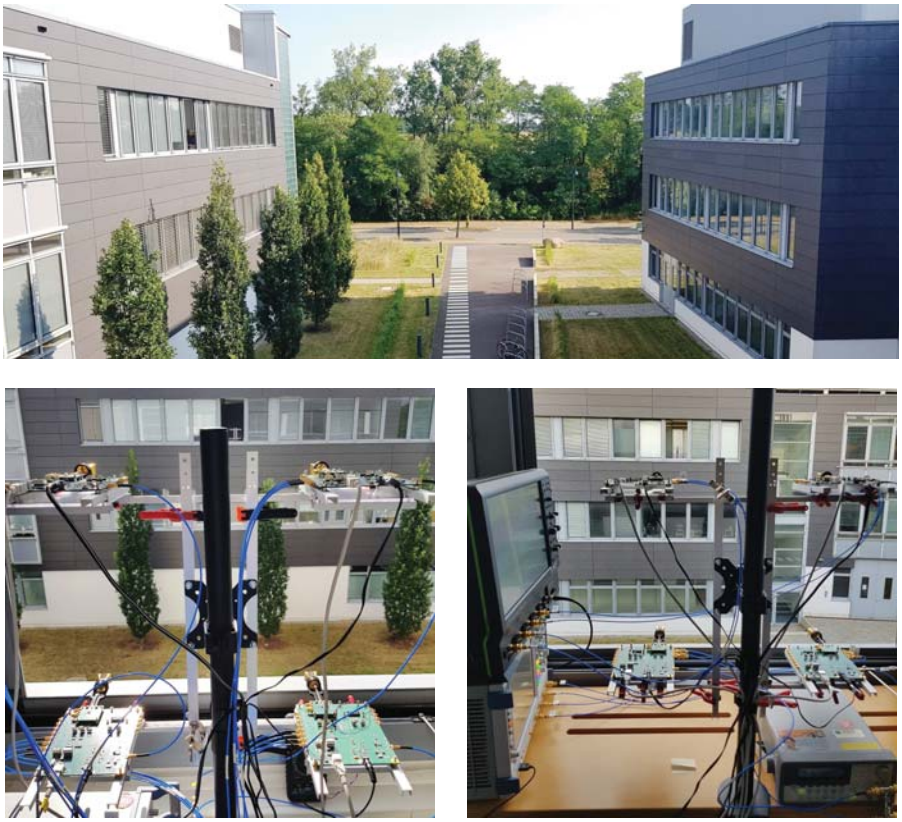

Figure 5.8
Backhaul LoS MIMO setup with $N_\mathrm{r} = N_\mathrm{t} = 4$ antennas, operating at a carrier frequency of 60.48 GHz and a link range of 21.1 m. From [230]

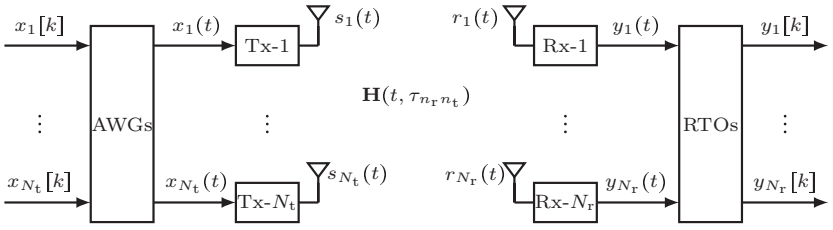

Figure 5.9
Basic system configuration used for the measurements, consisting of baseband signal generation and recording, using AWG and RTO, and Tx/Rx front ends with antennas. From [230]

eral optimal spacings that can be identified in the plot, we have selected $d_{\mathrm{LoS}} = 0.395\,\mathrm{m}$ for a compact measurement setup.

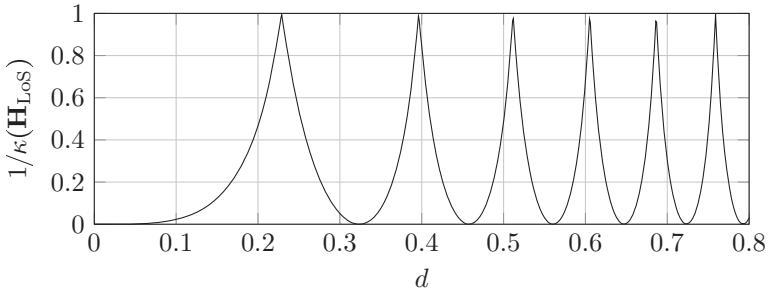

Figure 5.10
Inverse of the channel matrix condition number for different antenna spacings d under a 4×4 URA LoS MIMO setup at a carrier frequency of 60.48 GHz and link range of 21.1 m. A maximum theoretical value of 1 translates to a fully orthogonal channel matrix. From [230]

In the post-processing of the recorded measurements, channel estimation was performed using the correlation-based approach described in Section 5.4.1. For this purpose, mutually orthogonal 127-symbol long pseudo-random noise (PN) sequences with high auto-correlation and low cross-correlation properties were transmitted on the four different streams. The estimated condition number for the LoS MIMO component of the channel is $\mathrm{E}[\kappa(\hat{\mathbf{H}}_{\mathrm{LoS}})] \approx 2.2$, meaning that it is close to an orthogonal channel allowing for good spatial multiplexing. The difference of the estimated to the theoretical condition number can be attributed to several factors. Positioning errors in the antenna arrays in the order of millimeters can impair the channel orthogonality since the setup is sensitive to the antenna geometry. Furthermore, interference from possible reflections that falls within the LoS component of the channel would affect its conditioning as well.

In order to evaluate the presence of multipath components in the channel, we statistically analyzed the amplitude of the LoS versus the remaining interference taps. The results were taken from 2500 consecutive estimated channel impulse responses (CIRs), containing a total of 3.175×10^5 symbols, using the above described experimental setup. Prior to the tap analysis, the recording was normalized to the mean LoS path power and compensated for carrier frequency offset. By comparing the mean of tap distributions shown in Figure 5.11, we can conclude that the LoS tap is dominant and approx. 15 dB above the interference floor. It should be noted that there are several potential sources of interference in such a system setup. It can occur both due to the analog front-end's integration and the frequency-selectivity of its hardware components in wideband operation, as well as due to possible reflections in the propagation environment. Analog front-end calibration could

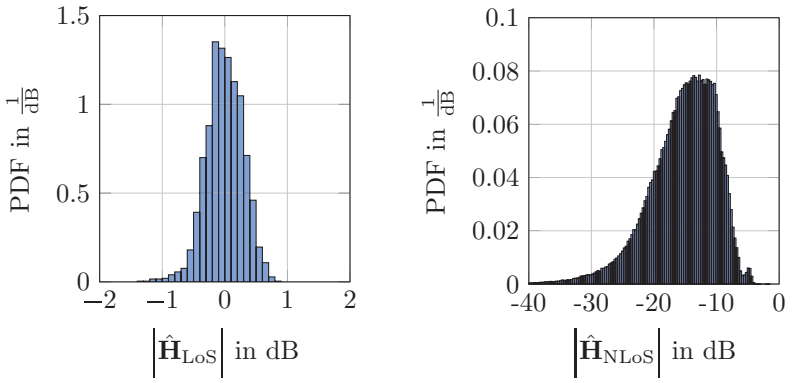

Figure 5.11
Amplitude distribution of (a) LoS channel taps, and (b) interference taps, taken from 2500 estimated CIRs for a 4×4 URA LoS MIMO setup at a carrier frequency of 60.48 GHz and link range of 21.1 m.

be performed to further reduce the interference floor to below -15dB and thus increase the link margin. Furthermore, the LoS tap can be considered stable in the long-term due to its low amplitude variation within ± 1 dB. Similar results were obtained in our previous measurement campaigns with 2×2 and 3×3 LoS MIMO setups reported in [232], thus confirming that near-orthogonal channels can be realized in environments with a strong LoS component.

5.6.3 Adaptive Equalization Results

In this section, equalization results for a $N_\text{r} = N_\text{t} = 4$ antenna LoS MIMO backhaul setup will be shown. The setup can be seen in Figure 5.8, where the separation between transmitter and receiver is 21.1 m. The carrier frequency of the system is 60.48 GHz and the symbol rate is 1.76 GBaud. Four independent and uncoded streams of 4-QAM modulated data were transmitted in a spatial multiplexing scheme. The sampling frequencies can be assumed synchronized, while for carrier frequency generation an independent oscillator setup was deliberately chosen.

An adaptive equalization structure, consisting of a feedforward filter of length $L_\text{R} = 10$ to combat interference, is chosen in order to equalize the channel and separate the streams. Since the MIMO channel is not perfectly orthogonal, the step size is chosen as $\mu_\text{F}/2$. The equalizer is initialized with an MMSE filter based on a channel estimate obtained through correlation, before decision directed tracking begins. The constellation diagrams after adaptive equalization of C consecutive symbols per stream can be seen in Figure 5.12. It is seen that the four streams can be well separated and that the CFOs are removed, yielding an average MSE of $10 \log_{10} \text{E}\left(\left|\mathbf{x} - \hat{\mathbf{x}}\right|^2\right) = 12.3\,\text{dB}$.

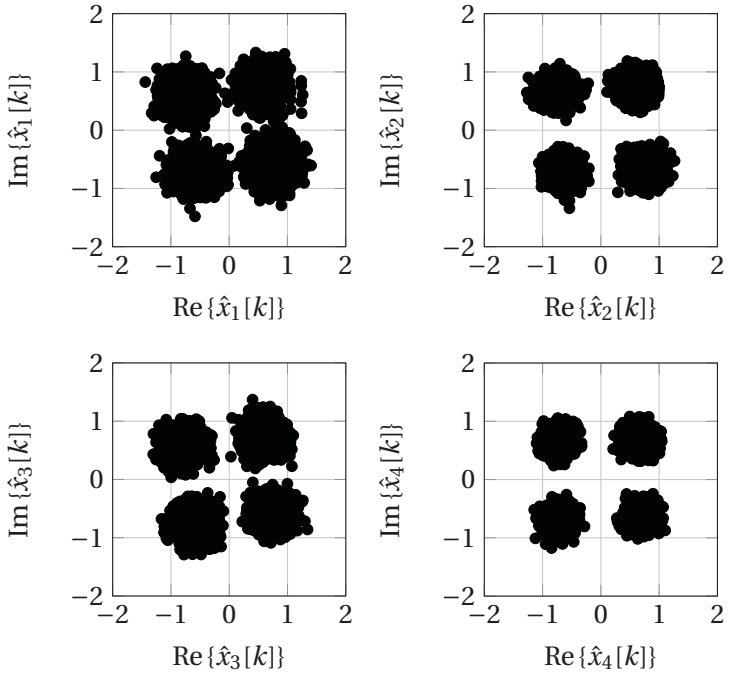

Figure 5.12
Constellation diagrams of the four estimated transmitted streams, with 1×10^4 symbols per stream, in the LoS MIMO setup shown in figure 5.9. Adaptive equalization with $\mu_F/2$ and a filter length of $L_R = 10$ was used. The average estimated MSE is 12.3 dB. From [230]

The achievable data rate with this setup is approximately 14 Gbit/s, and could potentially be increased by using a higher order modulation scheme like 16-QAM. Furthermore, the equalization performance may be improved by compensating I/Q imbalance through using a widely linear adaptive filter, or considering fractionally spaced equalizers also employing feedback, as mentioned in [213, 230]. In general this means roughly a tripling of the data rate compared to the two stream spatial multiplexing achieving approximately 5 Gbit/s with a symbol rate of 1.25 GBaud, which was achieved in [213].

5.7 Conclusion and Extensions

In this work we analyze the applicability of LoS spatial multiplexing at high carrier frequencies, e.g., in the mmWave frequency band, for ultra-high

throughput wireless backhaul applications. The wireless channel between the antenna arrays in strong LoS MIMO conditions is largely determined by the antenna topology. With optimally spaced antennas, orthogonal channels with full spatial multiplexing gain can be obtained in the ideal case. In [225] we show that the LoS-dominant MIMO channel matrix can be factorized into a product of three matrices with two diagonal matrices at outer positions. This channel factorization model can be used to derive antenna topologies with 1D/2D/3D structures, that are robust against antenna displacements. Potentially supporting data rates above 100 Gbit/s for wireless backhaul [219] and above 1 Tbit/s for wireless data bus [238] applications, this channel factorization also leads to a novel linear channel equalization method of reduced complexity that may become a key feature for systems of ultra-high symbol rates [207, 226, 213]. It was shown that compensating the effects of multiple frequency offsets is not a hindrance in MIMO systems. Correlation based estimators were proposed to measure the timing impairments, and two equalization structures were proposed. Adaptive equalization, being one of them, was shown to yield good results with relatively low complexity for mid to low CFOs.

Aiming for a practically feasible solution with low computational complexity, a lane-based receiver architecture with parallel baseband processing of the MIMO streams is proposed. By applying linear equalization algorithms such as ZF or SCE, it presents a viable approach that scales approximately linearly with the number of antennas [227]. In order to verify the proposed algorithms and the LoS MIMO channel conditioning at mmWave carrier frequencies, a 4×4 MIMO hardware-in-the-loop demonstration was performed in a backhaul-like scenario at 60 GHz. The measurements have confirmed that the LoS MIMO channel is near-orthogonal under the optimal antenna spacing, with an estimated condition number in the vicinity of two. Furthermore, a dominant LoS tap was observed, with approximately 15 dB separation from the interference components. With the given setup and applying adaptive equalization, a data rate of approx. 14 Gbit/s at an MSE of approx. 12.3 dB was demonstrated. Hence it was shown that mmWave LoS MIMO solutions are suitable for ultra-high throughput applications, where deterministic single-user links and high gain, but fixed, antenna radiation patterns are considered. In light of upcoming network developments, this work can be extended towards multi-user operation, where the users would also have the flexibility to direct the transmitted energy to certain directions of interest. Developing hybrid beamforming architectures with a good trade off between performance and hardware cost is therefore vital to unlock the full potential of multi-user LoS MIMO systems.